Finite Element Modeling of Microstructural Changes in Dry and Cryogenic Machining of *AZ31B* Magnesium Alloy for Enhanced Corrosion Resistance

Z. Pu
Institute for Sustainable Manufacturing,
University of Kentucky
Lexington, KY, USA

D. Umbrello
Department of Mechanical Engineering
University of Calabria
Rende, CS, Italy

D.A. Puleo
Center for Biomedical Engineering
University of Kentucky
Lexington, KY, USA

O.W. Dillon Jr, T. Lu, I.S. Jawahir,
Institute for Sustainable Manufacturing
University of Kentucky
Lexington, KY, USA

ABSTRACT
Unsatisfactory corrosion resistance is one of the major disadvantages of magnesium alloys that impede their wide application. Microstructural changes, especially grain sizes, of *Mg* alloys have significant influence on their corrosion resistance. Cryogenic machining was reported to effectively induce grain refinement on *Mg* alloys and has a potential to improve their corrosion resistance. It is important to model these changes so that proper machining conditions can be found to enhance the corrosion rate of *Mg* alloys. In this paper, a preliminary study was conducted to model the microstructural changes of *AZ31B Mg* alloy during dry and cryogenic machining using the finite element (FE) method and a user subroutine based on the dynamic recystallization (*DRX*) mechanism of *Mg* alloys. Good agreement in terms of grain size and affected layer thickness was found between experimental and predicted results. A numerical study was conducted using this model to investigate the influence of rake angle on microstructural changes after cryogenic machining.

KEYWORDS
Cryogenic Machining, Finite Element Method (FEM), Dynamic Recrystallization (*DRX*), Microstructrual Changes, *Mg* Alloy

INTRODUCTION

Mg alloys are potential lightweight materials for the transportation industry. They are also emerging as a promising candidate material for biodegradable metallic implants for cardiovascular and musculoskeletal applications [1, 2]. However, the unsatisfactory corrosion resistance of *Mg* alloys limits their application to a great extent, especially for biomedical applications where alloying and coating techniques are limited due to possible adverse tissue reactions.

Control of the microstructure, especially the grain size, has been proved to be an effective method to enhance the corrosion resistance of *Mg* alloys and this approach does not induce any undesirable chemical elements. Cryogenic burnishing reduced the grain size of *AZ31 Mg* alloy from 12 μm to 523 nm and remarkably improved its corrosion resistance in the 5% *NaCl* solution [3]. The critical influence of grain size on corrosion resistance was also reported on other materials and claimed to be analogous to the classical Hall–Petch relationship [4].

Machining is a severe plastic deformation (SPD) process and significant grain refinement was reported near the surface of various materials due to dynamic recrystallization (*DRX*), including *AISI 52100* steel [5] and *AZ31Mg* alloy [6]. "Affected layers", where remarkable grain refinement from 12 μm to 31 nm occurred, were found on the surface of *AZ31Mg* alloy after cryogenic machining and it was reported that cutting edge radius had an important influence on the thickness of the layer [6]. Cryogenic machining was reported to remarkably improve the corrosion resistance of machined samples in both 5 wt. % *NaCl* and simulated body fluid (*SBF*) [7]. Therefore, machining could provide a unique opportunity to adjust the corrosion resistance of *Mg* alloys if the grain size on the machined surface can be tailored by using proper machining conditions. A method to modulate the corrosion rate of *Mg*-based biodegradable fixation implants in the physiological environment is considered as a critical first step towards their successful application since fractured bones need different time to heal depending on the location, type of bones and health situation of different individuals [1].

In order to control the grain size after machining, it is important to have a reliable model which can predict the grain size changes after machining as a function of machining conditions. However, very limited research has been conducted to predict grain size changes in machining. A subroutine based on an empirical relationship between grain size and Zener-Hollomon parameter [8] during *DRX* was developed and implemented in DEFORM 2D to simulate the grain size changes in machining of *AISI 52100* [9] and *AA7075-T561* Alloy [10]. Dislocation density-based material models were developed to model grain size refinement and grain misorientation during orthogonal machining of commercially pure *Ti* [11]. There is no publication on modeling the grain size changes in machining of *Mg* alloys and current models do not include the cryogenic cooling conditions. The *AZ31 Mg* alloy is a good material to use to study *DRX* during machining since it does not undergo phase transformations when being cut.

In this study, a user subroutine based on empirical relationship between grain size and Zener-Hollomon parameter was developed and implemented in DEFORM 2D to predict the grain size changes on the machined surface of *AZ31B Mg* alloy under both dry and cryogenic conditions. An iterative procedure was utilized to calibrate the constants used in the subroutine using the experimental data. The results from numerical studies using the calibrated model on the influence of cooling methods, cutting edge radius and rake angle on microstructural changes were reported.

EXPERIMENTAL RESULTS

In order to calibrate and validate the FE model, orthogonal machining tests were conducted on *AZ31B Mg* alloy under both dry and cryogenic conditions. The details of the experimental study were reported elsewhere [6]. The machining tests were conducted on a Mazak Quick Turn-10 Turning Center using uncoated carbide tools with TNMG 432 geometry. For cryogenic machining, an Air Products ICEFLY® system was used to spray liquid nitrogen to the machined surface from the clearance side of the cutting tool as shown in Figure 1 (a). Forces and temperatures were recorded during the machining tests. The machining conditions tested are shown in Table 1. An example of affected layers formed after machining is shown in Figure 1 (b). The average grain size in the affected layer was 31 nm as shown in Figure 1 (c) while the initial grain size was 12 μm [6]. The thickness of the affected layer was dependent on the cooling method as well as cutting edge radius as shown in Table 1. The objective of the FE model is to predict the grain size as well as the thickness of the affected layer.

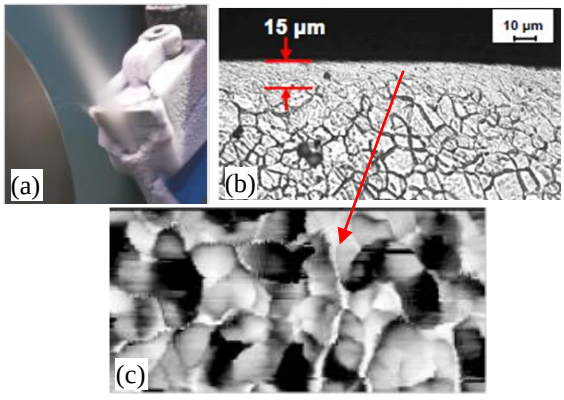

Figure 1. (a) Experimental setup for cryogenic machining , (b) affected layer formation and (c) AFM tapping mode phase image of the affected layer at about 2 μm from the surface after cryogenic machining [6].

NUMERICAL PROCEDURE

The mesh and boundary conditions for the FE model are shown in Figure 2. The temperatures at the bottom and left sides of the workpiece as well as the top and right sides of the cutting tool were set to equal to the room

temperature, T_{room}, which was 20 ℃. The top and right sides of the workpiece as well as the left and bottom sides of the cutting tool (marked by red lines in Figure 2) were allowed to exchange heat with the environment; the convection coefficient was 20 W/(m^{2}K), which is the default value for free air convection in DEFORM 2D (normally in the range of 5-25 W/(m^{2}K).

Table 1. Experiment matrix and affected layer thickness (cutting speed: 100 m/min; feed rate: 0.1 mm/rev) [6]

No.	Cooling Method	Cutting Edge Radius (μm)	Affected layer thickness (μm)
1	Dry	30	0
2	Cryogenic	30	8
3	Dry	70	20
4	Cryogenic	70	15

To simulate the effect of cryogenic cooling, an environmental window for heat exchange was defined as shown in Figure 2 and the width of the windows is 1 mm. The window is fixed in its position and does not move with the workpiece. The local convection coefficient in the window can be adjusted to simulate the cryogenic cooling effects and is one of the major parameter to be calibrated for modeling cryogenic machining.

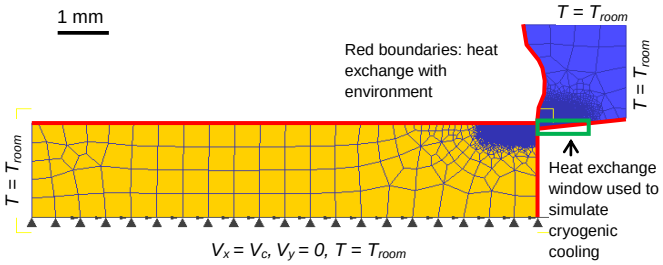

Figure 2. Mesh and boundary conditions for the FE model.

Material modeling

The physical and thermal properties of *AZ31B Mg* alloy used in the FE model are listed in Table 2 [12].

The Johnson–Cook constitutive equation was implemented in the FE code to model the material behavior of *AZ31B Mg* alloy during machining. The equation is:

$$\sigma = (A + B\cdot\varepsilon^{n})\cdot[1 + C\cdot\ln(\frac{\dot{\varepsilon}}{\dot{\varepsilon}_0})]\cdot[1-(\frac{T-T_{room}}{T_m-T_{room}})^{m}] \qquad (1)$$

where σ is the equivalent flow stress; ε is the equivalent plastic strain; $\dot{\varepsilon}$ is the equivalent plastic strain-rate (s^{-1}); $\dot{\varepsilon}_0$ is the reference equivalent plastic strain-rate (s^{-1}); T is the temperature of the work material; T_m is the melting temperature of the work material and T_{room} is the room temperature (20 ℃). In Equation 1, coefficient A is the yield strength (MPa); B is the hardening modulus (MPa); C is the strain-rate sensitivity coefficient; n is the hardening coefficient and m the thermal softening exponent.

Table 2. Physical and thermal material properties of *AZ31B Mg* alloy [12].

Melting temperature [K]	891
Young's Modulus [GPa]	45
Possion's ratio	0.35
Thermal Conductivity [W/(mK)]	77+0.096 T
Specific heat capacity [J/(kgK)]	1000+0.666T
Thermal expansion coefficient [K^{-1}]	2.48×10^{-5}

A wide range of mechanical tests of *AZ31B Mg* sheet was conducted under the strain-rates varied from 0.003 s^{-1} to 1500 s^{-1} and the temperature from room temperature to 250 ℃ [13]. After data fitting, the constants for the Johnson-Cook constitutive model were found for both rolling and transverse directions and are shown in Table 3 [13]. The average of the two directional values was used as the start values for the Johnson-Cook constants in the FE model. The values of *A* and *B* were adjusted slightly in the calibration process and will be explained in details in the corresponding section below.

Table 3. Initial Johnson-Cook constants of *AZ31B Mg* alloy used in the FE model [13]

	Rolling Direction	Transverse Direction	Average
A [MPa]	133.1	193.8	163.5
B [MPa]	345.8	296.8	321.3
n	0.293	0.380	0.337
C	0.016	0.016	0.016
m	1.849	1.808	1.829

It was shown that the machined chips of *AZ31B Mg* alloy under all the tested conditions were serrated [6]. Therefore, it is necessary to simulate the chip serration process in the FE model in order to accurately predict the forces and temperatures. There are two types of approaches that are utilized to simulate serrated chip formation.

The first approach is by using damage or material failure models together with the standard Johnson-Cook

material model [14, 18]. It is assumed that by using this method the chip segmentation occurred by crack initiation at critical points which is then followed by propagation inside the primary shear zone. The other approach to simulate serrated chips is to use a modified material flow stress model incorporating "flow softening" effects. Flow softening is due to microscopic level changes and is represented by a decrease in stress with increasing strain beyond a critical strain value. Below that critical strain, the material exhibits strain hardening. The standard Johnson-Cook material model agrees well with the material flow stress curves obtained from Split-Hopkinson Pressure Bar Test. However, it is noted that the levels of strain, strain-rate and temperature achieved with this experimental method are lower than the actual values that occur during the machining. The achievable maximum strain by the Split-Hopkinson Pressure Bar is about 0.5 and strain-rate is about 10^3 s^{-1} [14] while the actual machining process involves large shear strain (typically 2–10) and higher strain-rates (up to 10^6 s^{-1}) rates. For simulations outside the experimental range, the standard Johnson-Cook model is extrapolated and the flow stress will keep increasing with increased strain which was proved wrong by several researchers. These researchers reported that the flow stress decreased after the strain reached a critical value in *Ti* alloys [15]. The flow softening of *Ti* alloys was found to be caused by *DRX* [16]. The second approach of incorporating flow softening has become more popular recently due to the increased understanding of the material behaviors, especially on *Ti* alloys where large amount of material testing data has been reported. The second approach is also preferred by the authors since *DRX* is proved to occur during machining of *AZ31B Mg* alloy [6] and should be the cause for work softening. However, due to the limitation of the existing material testing data on *Mg* alloys, it was not possible at this time to develop a good material constitutive model incorporating *DRX* effects. Therefore, the first approach is used in the current study. The Cockroft and Latham's fracture criterion [17] were reported to successfully simulate the formation of serrated chips in machining *Ti* alloys [18]. This criterion is used in the current study and is expressed as:

$$\int_0^{\bar{\varepsilon}_f} \sigma_1 d\bar{\varepsilon} = D \qquad (2)$$

where $\bar{\varepsilon}_f$ is the effective strain; σ_1 is the maximum principal stress; *D* is a value calculated for each element by DEFORM for each step by using Equation 2. When the calculated *D* value of any elements is larger than $D_{critical}$, which is a material constant, the flow stress of these elements is forced to be only 10% of the original value, which is the stress calculated using Equation 1. The DEFORM software automatically reduced the flow stress of those elements whose calculated *D* values are larger than $D_{critical}$ to 10% of the original flow stress. This forced reduction of flow stress crudely simulates the "flow softening" induced by *DRX*. It is expected that by calibration of the material constants using the experimental data, a reasonable agreement between the FE model and the measured data on force, temperature and chip morphology can still be achieved. More details on the changes of *D* during a chip segmentation cycle were reported elsewhere [7].

Friction model

The influence of different tool-chip friction models on FEM results was investigated by Filice et al. [19] and it was found that as long as the friction coefficient was well calibrated, both cutting forces and chip morphology could be well predicted independent of which friction model was used. In this study, a simple constant shear friction model is applied:

$$\tau = \mu \cdot \tau_0 \qquad (3)$$

where τ is the frictional stress between the tool and the chip and work material, τ_0 is the shear flow stress of the work material and μ is a friction coefficient. It was reported that the application of liquid nitrogen decreased the friction coefficient in a contact sliding friction test [20], especially when the contact force was low (200-300 N). However, the test was conducted at room temperature which is different than the actual machining environment. The influence of cryogenic cooling on friction coefficient was not well reported by other literature. In the present study, the same friction coefficient was used for both dry and cryogenic machining.

FE MODEL CALIBRATION AND VALIDATION

The objective of the model in this study is to predict grain size changes after dry and cryogenic machining using a user subroutine in DEFORM 2D software. Before the development of the subroutine, it is important to establish a calibrated and validated model in terms of forces, temperature as well as chip morphology.

The calibration process of the FE model for machining *AZ31B Mg* alloy is shown in Figure 3. The values of the friction coefficient μ and the critical damage value $D_{critical}$ were determined through an iterative calibration process using the experimental data on cutting forces and chip morphology from dry machining with a 30 μm edge radius tool. The heat transfer coefficient h_{int} at the tool-chip interface was fixed at 1000 kW/ (m^2 K) at this stage of calibration; this value was used by several researchers and good agreement with experimental data was reported [19]. The studied range for μ was from 0.1 to 0.7. The initial estimated value of $D_{critical}$ was found by integrating

a published flow stress curve of *AZ31B Mg* alloy from beginning of deformation to fracture [13]. It was found that the best agreement in cutting force was achieved (7% difference between the experiment and predicted values) when the values of $D_{critical}$ and μ were 35 and 0.7, respectively. The predicted thrust forces were 8% smaller than the experimental results which agree with most literature that FE models tended to underestimate the thrust forces [19].

It is reported that the thrust force has a dominant influence on the microstructural changes of the workpiece [6]. Therefore, the accurate prediction of the thrust force is of relatively more importance than the cutting force. Possible cause for the underestimate of thrust forces in FE models could be the oversimplified material model which does not take *DRX* into consideration. The differences between the material testing conditions where the constants were obtained and the actual conditions involved in a machining is another possibility. After slightly adjusting the Johnson-Cook constants *A* and *B* to *A* = 200 MPa and *B* = 400 MPa, the difference between the predicted thrust force and the experimental one is reduced from 8% to 3.1%. At the same time, the prediction of the cutting force is still in reasonable range (less than 12%).

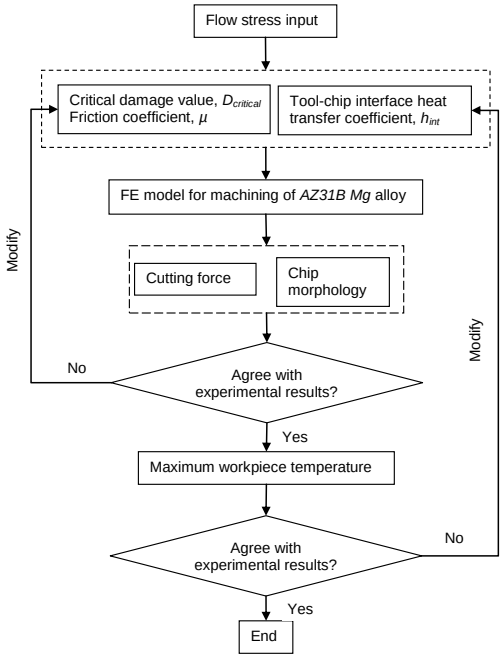

Figure 3. Flow chart for the calibration of the FE model for machining *AZ31B Mg* alloy.

In addition to forces, good agreement of chip morphology was achieved when the values of $D_{critical}$ and μ were 35 and 0.7, respectively. A comparison between experimental data and predicted values is shown in Figure 4. The differences range from 10% to 20%. Since there is no known correlation between the affected layers on the workpiece and the chip morphology, the importance of chip morphology calibration is less than forces and temperature and this level of differences are deemed adequate.

Temperature is proved to be one of the most important factors that cause the microstructural changes of the machined surface [6]. A two step calibration of the FE model was conducted to find the values of heat transfer coefficients. First, the heat transfer coefficient at the tool-chip interface h_{int} was determined through an iterative process using the temperature measurement data from dry machining using the 30 μm tool. Then the value of h_{int} was fixed and the convection coefficient h_{cryo} of the local environment window defined in Figure 2 was determined through another iterative process using the temperature measurement data from cryogenic machining using the 30 μm tool.

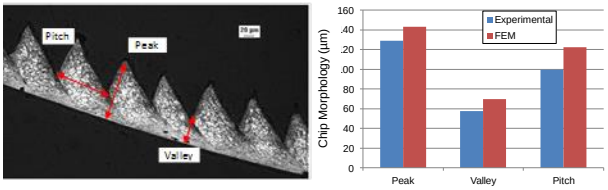

Figure 4. Definition of chip morphology (a) and comparison between predicted and experiment data after dry machining with a 30 μm edge radius tool (V = 100 m/min, f = 0.1 mm/rev).

It was found that when the initial choice of h_{int} value of 1000 kW/ (m^2 K) was used the maximum temperature on the workpiece was about 180 ℃, which was higher than the measured value of 125 ℃. A good agreement between the predicted and measured temperature was achieved when the h_{int} value was increased to 5000 kW/ (m^2 K). Figure 5 (a) shows the predicted temperature distribution on the workpiece for dry machining with a 30 μm edge radius tool when the h_{int} value of 5000 kW/ (m^2 K) was used. The temperature starting from the start point of the newly formed surface along the workpiece was measured in the FE model and shown in Figure 5 (d). The temperature gradually drops with increased distance from the start point and the maximum temperature is 135 ℃, about 8% higher than the measured value.

To simulate the cryogenic cooling effects, the local heat exchange window was used as shown in Figure 2. The width of the widows is 1 mm which is assumed to the contact length between the machined surface and the liquid nitrogen jet. This use of the window only change the convection coefficient of the machined surface which is covered by the window from the initial value of 20 kW/ (m^2 K) to the value of h_{cryo}. The window does not change any other boundary conditions in the FE model. Figure 5 (b) and (c) show the predicted temperature distributions during cryogenic machining when different convection

coefficients were used within the window. A good agreement with measured temperature was achieved when the convection coefficient h_{cryo} was set to 5000 kW/(m^{2}K). The predicted maximum temperature on the machined surface was 51 ℃, about 2% lower than measured value.

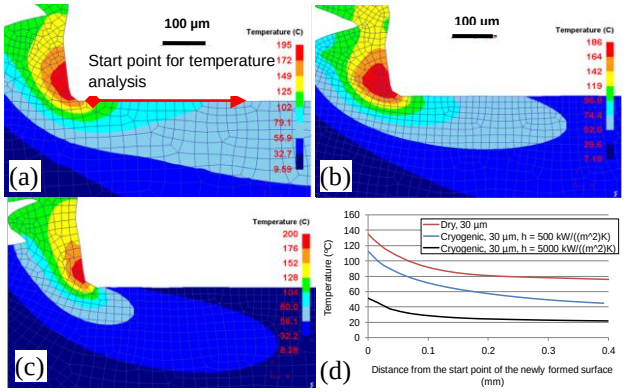

Figure 5. Predicted temperature distribution for (a) dry machining, (b) cryogenic machining with h_{cryo} = 500 kW/(m^{2}K), (c) cryogenic machining with h_{cryo} = 5000 kW/(m^{2}K) and (d) predicted temperature profiles along the machined surface under different conditions (r_n = 30 µm, V = 100 m/min, f = 0.1 mm/rev, h_{int} =1000 kW/ (m^2 K)).

Validation of the FE model

After the calibration process was completed, the important constants in the FE model were determined as shown in Table 4. The only difference in terms of constants used to simulate dry and cryogenic machining is the convection coefficient in the local heat exchange window, h_{cryo}. All the other constants have the same value for dry and cryogenic machining. To evaluate the performance of the calibrated FE model, machining simulations under different edge radii and cooling conditions were conducted and compared with the experimental data [6] . Two factors that have critical influence on the microstructural changes were considered for the validation, thrust force and temperature.

Figure 6 (a) shows the comparison of measured and predicted forces under dry and cryogenic conditions (V = 100 m/min, f = 0.1 mm/rev). The measured data on dry machining with the 30 µm edge radius tools was used for calibration and all the other three conditions were used for validation purpose. Good agreements between the measured and predicted thrust forces were achieved. The maximum difference is 4%. The cutting forces were not as important as thrust force in the present study since the latter one directly relates with the influenced layer thickness of microstructural changes. The predicted cutting forces were overestimated in most cases. The maximum error is 19% when the 70 µm edge radius tools were used under cryogenic conditions.

Table 4. Summary of important constants used in the FE model

Johnson-Cook constants	A = 200 MPa, B = 400 MPa, n = 0.337, C = 0.016, m = 1.829
Critical damage value, $D_{critical}$	35
Friction coefficient, μ	0.7
Heat transfer coefficient at the tool-chip interface, h_{int} (For both dry and cryogenic conditions)	5000 kW/ (m^2 K)
Convection coefficient in the local heat exchange window, h_{cryo} (For cryogenic condition only)	5000 kW/ (m^2 K)

Figure 6 (b) shows the comparison of measured and predicted maximum workpiece temperature under dry and cryogenic conditions (V = 100 m/min, f = 0.1 mm/rev). The predicted data on cryogenic machining with the 70 µm edge radius tools was used for validation purpose. The difference between the predicted and measured temperature is 7% which shows that the FE model is capable of temperature prediction.

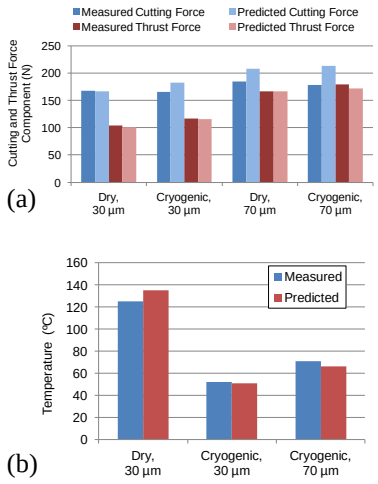

Figure 6. Comparison of (a) measured and predicted forces and (b) maximum workpiece temperature with different cutting edge radii under dry and cryogenic conditions (V = 100 m/min, f = 0.1 mm/rev).

User Subroutine Calibration

In order to predict the grain size and affected layer thickness after machining, it is important to understand the mechanism for the grain refinement. It has been shown that the significant grain refinement was induced by dynamic recrystallization (*DRX*) [6]. The critical conditions for the onset of *DRX* in *AZ31 Mg* alloy in

standard material property testing were investigated by several researchers [21, 22]. For *DRX* to occur, a critical strain, ε_{cr}, needs to be reached. This critical strain value was found to be dependent on the strain-rate and temperature [22]. It can be calculated using the Zener-Hollomon parameter, *Z*, as:

$$\varepsilon_{cr} = 0.02039 Z^{0.06} \quad (4)$$

Z is defined as:

$$Z = \dot{\varepsilon} \times \exp(\frac{Q}{RT}) \quad (5)$$

where ε̇ is the strain-rate; *Q* is the activation energy; *R* is the gas constant and *T* is the temperature.

An empirical formula was used to predict the size of the recrystallized grains in *AZ31 Mg* alloy after friction stir processing with the application of liquid nitrogen, and this was proved to be consistent with the experimental results [23]. The formula is:

$$\frac{d_{rec}}{d_{init}} = 10^3 \times Z^{-1/3} \quad (6)$$

where d_{rec} is the recrystallized grain size; d_{init} is the initial grain size.

In the user subroutine, when the calculated strain in the workpiece exceeds the critical strain, the initial grain size, d_{init}, is replaced with the grain size after *DRX*, d_{rec}, which can be calculated by Equation 6. This calculation is carried out continuously for every element in the workpiece for each step.

The constants in Equation 4 and Equation 6 were found in the same workpiece material but different manufacturing processes. Therefore, it is expected these constants to be calibrated using the experimental results before the subroutine can accurately predict the formation of affected layers induced by machining. The flowchart for the calibration of the subroutine is shown in Figure 7. The exponents in Equation 4 and Equation 6 were found to be the most important constants (referred to as *a* and *b*, respectively, in Figure 7) and were determined by an iterative calibration process.

Figure 8 shows the variation of predicted strain and critical strain with distance below the machined surface before calibration for cryogenic machining with the 70 μm edge radius tools. The data was taken from 0.1 mm away from the start point of the newly formed machined surface as shown in Figure 9 (a). It shows that the predicted recrystallized layer is more than 50 μm thick when the original value a = 0.06 was used, which is much larger than the measured value (15 μm). It can be found from Figure 8 that the critical strain at the depth of 15 μm needs to be equal to 1.9 in order to have a recrystallized layer with the thickness of 15 μm (ε_{cr} = 1.9). Since the Zener-Hollomon parameter at the depth of 15 μm can also be calculated using the calibrated FE model, the exponent in Equation 4 can be found. The exponent, *a*, was increased from 0.06 to 0.075 to improve agreement with experimental data. The predicted grain size on the surface was found to be about 50 nm, which is slightly larger than the measured 31 nm. After calibration, the exponent in Equation 6 was found to be -0.205.

The predicted grain size distributions after calibration under different machining conditions are shown in Figure 9. Only the experiment data from cryogenic machining with the 70 μm edge radius tool was used for the calibration and all the data in the other three groups were used for validation. It shows that good agreement was achieved between the predicted grain size and the measured data.

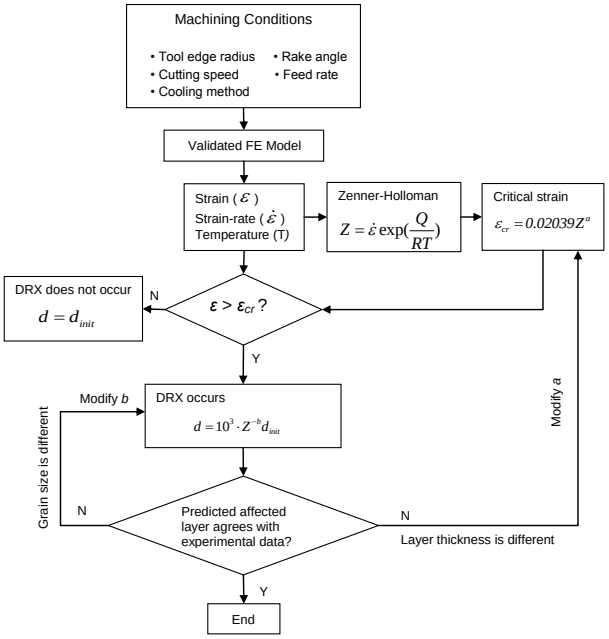

Figure 7. Flow chart for the calibration of the user subroutine to predict the affected layer on the machined surface.

For both dry and cryogenic conditions, machining with the larger edge radius tool led to the formation of thicker grain refinement layers. The data on variation of grain size with depth below the machined surface was extracted at the location 0.1 mm away from the start point of newly formed surface (the point where the workpiece leaves the cutting edge) as shown in Figure 9 (a). Figure 10 (a) shows the variation of grain size with depth below the machined surface under different machining conditions. Grain refinement on the surface and sub-surface was successfully predicted by the user subroutine. The predicted grain size within the first 12 μm on the machined surface after cryogenic machining using the 70 μm edge radius tool is about 40 nm, which is very close to the measured grain size of 31 nm. The sudden increase of

grain size after 12 µm is very similar to the observed microstructure in Figure 1 (b) where a clear interface between the affected layer and the bulk material is shown.

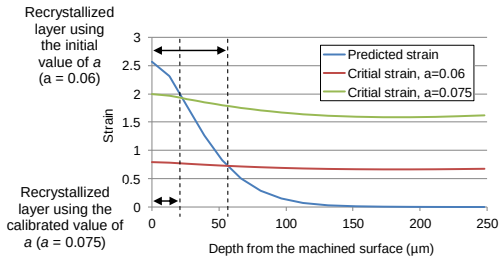

Figure 8. Variation of predicted strain and critical strain with distance from the machined surface before and after calibration of exponent a in Equation 4 (cryogenic, r_n = 70 µm, V = 100 m/min, f = 0.1 mm/rev).

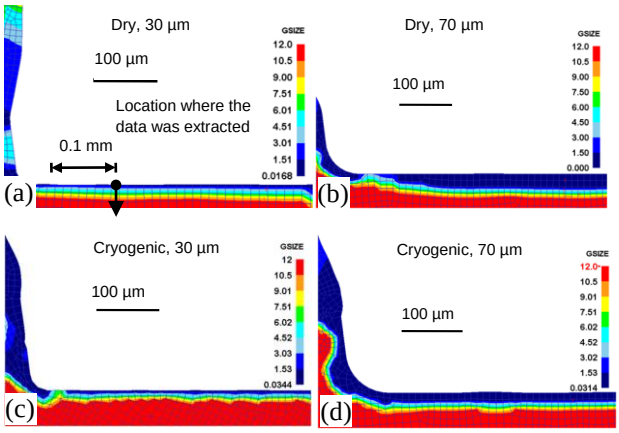

Figure 9. Predicted grain size distribution after machining using different cooling methods and tools with various edge radii (V = 100 m/min, f = 0.1 mm/rev).

Figure 10 (c) shows the grain size on the machined surface. The influence of cryogenic cooling on grain size is predicted to be dramatic, which agrees with the experimental results [6]. For both edge radii, cryogenic cooling results in significantly smaller grain size. It is assumed that the grain size in the affected layer is smaller than 2 µm which approaches the limit of the optical microscope used in the study. Therefore, the thickness of the predicted affected layers can be measured from Figure 10 (a). Edge radius does not play an important role in determining the grain size on the machined surface but has remarkably influence on the thickness of the affected layers as shown in Figure 10 (d). This agrees with the finding from the experimental data shown in Table 1. The predicted thickness of the affected layer on machined surface after cryogenic machining using the 70 µm edge radius tool is 15.4 µm which agrees well with the measured value. The predicted value for dry machining using the 70 µm edge radius tool is 28.8 µm and is a little larger than the measured value (20 µm). This may be due to the fact that the user subroutine does not take into consideration of grain growth after *DRX*. Figure 11 (a) shows the variation of predicted temperature with depth from the machined surface under different machining conditions. It shows the temperatures within the first 80 µm from the machined surface under cryogenic conditions are significantly lower than those under dry conditions. The surface temperature under cryogenic cooling was less than 30% of that under dry conditions when the 30 µm edge radius tools were used. This predicted data trend agrees well with the temperature measurement [6]. Therefore, it is highly possible that a certain amount of grain growth occurs after *DRX* during dry machining and in turn this leads to the reduction of thickness of the affected layer. This claim was also supported by the study [24] which reported that ultrafined/nano grain structure were only found on the top of the machined surface of copper when the cutting speed was very low (< 3 m/min) during dry machining.

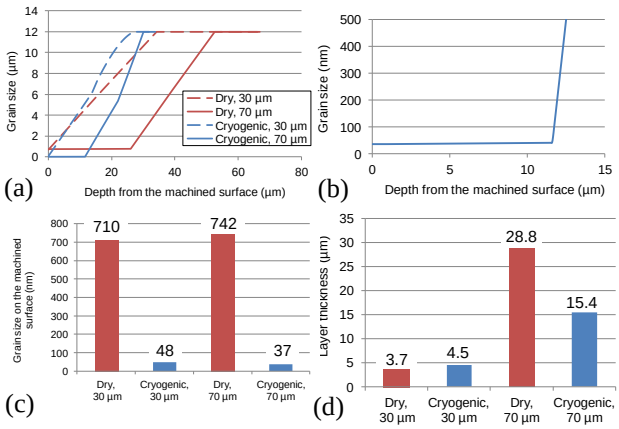

Figure 10. (a) Predicted variation of grain size with depth below the machined surface; (b) enlarged view on the machined surface after cryogenic machining with the 70 µm edge radius tool; (c) predicted grain size on the machined surface and (d) thickness of the affected layers under different machining conditions (V = 100 m/min, f = 0.1 mm/rev).

Although no affected layer was observed in the experiments on the machined surface after dry machining using the 30 µm edge radius tool, it is possible that a very thin grain refinement layer formed and it cannot be recognized by the optical microscope used in the study. The user routine predicted that the affected layer under these conditions is 3.7 µm. The predicted thickness of the affected layer on the workpiece after cryogenic machining using the 30 µm edge radius tool is 4.5 µm, which is smaller than the measured value of 8 µm. These differences could be caused by the size of the used element since the average element dimension is about 10

μm and is larger than the thickness of the affected layer under this condition. The increase of the thickness under cryogenic conditions compared with dry conditions could be caused by the increased strain as shown in Figure 11 (b). Cryogenic cooling leads to 40% increase in strain when the 30 μm edge radius tool was used. Much smaller difference in the strain was observed when the 70 μm edge radius tool was used.

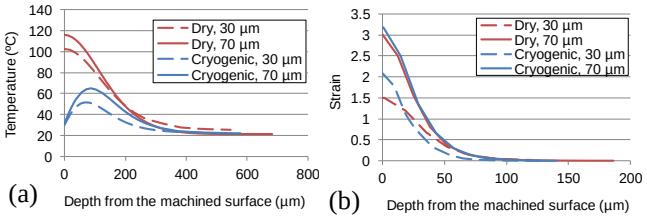

Figure 11. Variation of (a) predicted temperature and (b) strain with depth from the machined surface under different machining conditions (V = 100 m/min, f = 0.1 mm/rev).

FE ANALYSIS

The calibrated user routine can predict reasonably well the grain size distribution on the surface and sub-surface of the machined workpiece. In this section, this user subroutine will be used to investigate the influence of rake angle on the formation of the affected layers as well as key *DRX* factors, such as strain and temperature on the workpiece. The cooling conditions for all the simulations are cryogenic cooling and the edge radius of the cutting tools are 70 μm.

Rake angle of the cutting tools was proved experimentally to have a remarkable influence on the plastic deformation of the machined surface and sub-surface [24]. The plastic strain on the brass surface machined with a -30° rake angle tool was 3 times larger than that machined with a +10° rake angle tool [24]. Figure 12 (a) shows the predicted grain size and affected layer thickness under different rake angles. The thickest affected layer (29 μm) was obtained when using the most negative rake angle and using positive rake angle results in the thinnest layer (3 μm). The predicted strains on the workpiece under different rake angles are shown in Figure 12 (b). Machining using a -30° rake angle led to 125% increase of the surface strains compared with using a + 20° rake angle, which agrees with the literature [24] and is the cause for increased thickness of the affected layer. The predicted grain size on the machined surface is shown in Figure 12 (a). Machining using a positive rake angle resulted in much larger grain size on the surface. This could be caused by the fact that positive rake angles induce less deformation on the workpiece and lower strain-rate. Since the difference in temperature is much smaller than the one in plastic deformation as shown in Figure 12, machining with a positive rake angle could lead to a smaller Z value and therefore increase the grain size after *DRX*. The difference in temperature is much larger than the plastic strains on the machined surface when the rake angle was changed from -7 ° to -30 ° as shown in Figure 12; this likely is the cause for the larger grain size when a more negative rake angle was used.

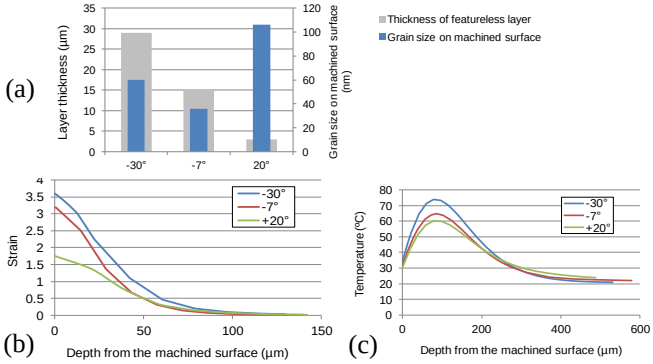

Figure 12. A comparison of (a) affected layer thickness and grain size on the surfaces machined under different rake angles; variation of (b) predicted strain and (c) temperature with depth from the surface machined under different rake angles (cryogenic, r_n = 70 μm, V = 100 m/min, f = 0.1 mm/rev).

CONCLUSIONS

A FE model was developed to simulate the machining of *AZ31B Mg* alloy using the commercial software DEFORM 2D under both dry and cryogenic conditions. The comparison between initial predictions and experimental data on forces and temperature as well as chip morphology was used to calibrate the FE model by updating the model parameters. A user subroutine was developed to predict the formation of affected layers induced by machining based on the dynamic recystallization (*DRX*) mechanism of *AZ31B Mg* alloys. After evaluation using the experimental data, the user subroutine successfully predicted the formation of affected layers under various cutting conditions, including different cooling methods, tool edge radius and rake angle. Also, critical *DRX* parameters, such as strain and temperature, on the machined surface and sub-surface were predicted by the FE model. With further development and validation, the model can be used to provide cutting conditions for manufacturing of *Mg*-based fixation implants with tailored biodegradable rates.

ACKNOWLEDGEMENTS

This work was funded by and conducted in the Institute of Sustainable Manufacturing at the University of Kentucky, USA. The authors would like to thank Air

Products and Chemicals for providing the ICEFLY® liquid nitrogen delivery system.

REFERENCES

[1] Staiger, M. P., Pietak, A. M., Huadmai, J., and Dias, G., 2006, Magnesium and its alloys as orthopedic biomaterials: A review, Biomaterials, 27(9), pp. 1728-1734.

[2] Denkena, B., and Lucas, A., 2007, Biocompatible Magnesium Alloys as Absorbable Implant Materials – Adjusted Surface and Subsurface Properties by Machining Processes, CIRP Annals - Manufacturing Technology, 56(1), pp. 113-116.

[3] Pu, Z., Song, G. L., Yang, S., Outeiro, J. C., Dillon, O. W., Puleo, D. A., and Jawahir, I. S., 2012, Grain refined and basal textured surface produced by burnishing for improved corrosion performance of AZ31B Mg alloy, Corros Sci, 57, pp. 192-201.

[4] Birbilis, N., Ralston, K. D., and Davies, C. H. J., 2010, Revealing the relationship between grain size and corrosion rate of metals, Scripta Mater, 63(12), pp. 1201-1204.

[5] Ramesh, A., Melkote, S. N., Allard, L. F., Riester, L., and Watkins, T. R., 2005, Analysis of white layers formed in hard turning of AISI 52100 steel, Mat Sci Eng a-Struct, 390(1-2), pp. 88-97.

[6] Pu, Z., Outeiro, J. C., Batista, A. C., Dillon, O. W., Puleo, D. A., and Jawahir, I. S., 2012, Enhanced surface integrity of AZ31B Mg alloy by cryogenic machining towards improved functional performance of machined components, Int J Mach Tool Manu, 56, pp. 17-27.

[7] Pu, Z., 2012, Cryogenic Machining and Burnishing of AZ31B Magnesium Alloy for Enhanced Surface Integrity and Functional Performance, University of Kentucky.

[8] Yanagimoto, J., Karhausen, K., Brand, A. J., and Kopp, R., 1998, Incremental formulation for the prediction of flow stress and microstructural change in hot forming, J Manuf Sci E-T Asme, 120(2), pp. 316-322.

[9] Caruso, S., S. Renzo, Umbrello, D., Jayal, A. D., Dillon, O. W., and Jawahir, I. S., 2011, Finite Element Modeling of Microstructural Changes in Hard Turning, Advanced Materials Research, 223, pp. 960-968.

[10] G. Rotella, L. S., D. Umbrello, O.W. Dillon Jr, I.S. Jawahir, 2012, Finite Element Modeling of Microstructural Changes in. Turning of AA7075-T651 Alloy and Validation, Journal of Manufacturing Processes, 15, pp. 87-95.

[11] Ding, H., and Shin, Y. C., 2011, Dislocation Density-Based Grain Refinement Modeling of Orthogonal Cutting of Commercially Pure Titanium, ASME Conference Proceedings, 2011(44311), pp. 89-98.

[12] Hibbins, S. G., 1998, "Investigation of Heat Transfer in DC Casting of Magnesium Alloys," Proceedings of the International Symposium on Light Metals, M. Sahoo, and C. Fradet, eds.Calgary, AB, Canada, pp. 265-280.

[13] Hasenpouth, D., 2010, Tensile High Strain Rate Behavior of AZ31B Magnesium Alloy Sheet, University of Waterloo, Waterloo, Ontario, Canada.

[14] Calamaz, M., Coupard, D., and Girot, F., 2008, A new material model for 2D numerical simulation of serrated chip formation when machining titanium alloy Ti-6Al-4V, Int J Mach Tool Manu, 48(3-4), pp. 275-288.

[15] Miller, R. M., Bieler, T. R., and Semiatin, S. L., 1999, Flow softening during hot working of Ti-6Al-4V with a lamellar colony microstructure, Scripta Mater, 40(12), pp. 1387-1393.

[16] Ding, R., and Guo, Z. X., 2004, Microstructural evolution of a Ti–6Al–4V alloy during β-phase processing: experimental and simulative investigations, Materials Science and Engineering: A, 365(1–2), pp. 172-179.

[17] Cockcroft, M. G., and Latham, D. J., 1968, Ductility and workability of metals, Journal Institute of Metals, 96 pp. 33-39.

[18] Umbrello, D., 2008, Finite element simulation of conventional and high speed machining of Ti6Al4V alloy, J Mater Process Tech, 196(1-3), pp. 79-87.

[19] Filice, L., Micari, F., Rizzuti, S., and Umbrello, D., 2007, A critical analysis on the friction modelling in orthogonal machining, Int J Mach Tool Manu, 47(3-4), pp. 709-714.

[20] Hong, S. Y., Ding, Y., and Jeong, J., 2002, Experimental evaluation of friction coefficient and liquid nitrogen lubrication effect in cryogenic machining, Machining Science and Technology, 6(2), pp. 235-250.

[21] Huang, G., Qian, B., Wang, L., and Jonas, J. J., 2007, Study on the critical conditions for initial dyanmic recrystallization of AZ31 Magnesium alloy, Rare Metal Materials and Engineering, 36, pp. 2080-2083.

[22] Wang, L., Huang, G., and Fan, Y., 2002, Investigation on hot deform ation behavior of AZ31 magnesium, Journal ofChongqing University-English Edition, 1, pp. 57-59.

[23] Chang, C. I., 2007, Achieving Ultrafine Nano Grains in AZ31 Mg Based Alloys and Composites by Friction Stir Processing, Sun Yat-Sen University.

[24] Chandrasekar, S., Calistes, R., Swaminathan, S., Murthy, T. G., Huang, C., Saldana, C., and Shankar, M. R., 2009, Controlling gradation of surface strains and nanostructuring by large-strain machining, Scripta Mater, 60(1), pp. 17-20.